Primitive quantum gates for an math xmlns="http://www.w3.org/1998/Math/MathML" display="inline">mi>S/mi>mi>U/mi>mo stretchy="false">(/mo>mn>2/mn>mo stretchy="false">)/mo>/math> discrete subgroup: Binary tetrahedral

Erik J. Gustafson, Henry Lamm, Felicity Lovelace, and Damian Musk

Primitive Quantum Gates for an $SU(2)$ Discrete Subgroup: $\mathbb{BT}$

Erik J. Gustafson,[1, *] Henry Lamm,[1, †] Felicity Lovelace,[2, ‡] and Damian Musk[3, §]

[1]*Fermi National Accelerator Laboratory, Batavia, Illinois, 60510, USA*
[2]*Department of Physics, University of Illinois at Chicago, Chicago, Illinois 60607, USA*
[3]*Stanford University Online High School, Redwood City, CA 94063, USA*
(Dated: November 2, 2022)

We construct a primitive gate set for the digital quantum simulation of the binary tetrahedral ($\mathbb{BT}$) group on two quantum architectures. This nonabelian discrete group serves as a crude approximation to $SU(2)$ lattice gauge theory while requiring five qubits or one quicosotetrit per gauge link. The necessary basic primitives are the inversion gate, the group multiplication gate, the trace gate, and the $\mathbb{BT}$ Fourier transform over $\mathbb{BT}$. We experimentally benchmark the inversion and trace gates on `ibm_nairobi`, with estimated fidelities between $14-55\%$, depending on the input state.

I. INTRODUCTION

Simulating the dynamics of lattice field theories offers a clear potential for quantum advantage [1–6]. Time evolution on quantum computers requires efficiently implementing the unitary operator $U(t) = e^{-iHt}$. Various approximations for $U(t)$ with different tradeoffs exist [3, 7–18], but all of them require implementing key group theoretic operations as quantum circuits in the case of lattice gauge theories [19]. This separation of the problem into group-dependent primitives [20] and algorithmic design [21] has proven fruitful in optimizing both.

For efficient digital simulations, many proposals exist on how the lattice gauge degrees of freedom can be truncated [7, 22–61]. For some regulated theories, the desired theory may not even be the true continuum limit [50, 51, 53, 62–69]. Furthermore, the relative efficacy of schemes is dimension-dependent [20, 45, 70].

One promising digitization method is the discrete subgroup approximation [7, 31–35, 56, 71, 72]. This method was explored early on in Euclidean lattice field theory to reduce resources. Replacing $U(1)$ by $\mathbb{Z}_N$ was considered in [73, 74]. Extensions to the crystal-like subgroups of $SU(N)$ were made in Refs. [31, 32, 56, 75–80], including with fermions [81, 82]. Theoretical studies revealed that the discrete subgroup approximation corresponds to continuous groups broken by a Higgs mechanism [83–87]. On the lattice, this causes the discrete subgroup to poorly approximate the continuous group below a *freezeout* lattice spacing a_f (or beyond a coupling β_f).

Lattice calculations are performed at fixed lattice spacing $a = a(\beta)$ which approaches zero as $\beta \to \infty$ for asymptotically free theories. Finite a leads to discrepancies from the continuum results, but provided one simulates in the *scaling regime* below $a_s(\beta_s)$, these errors should be polynomial in a. Any approximation error from using discrete subgroups should be tolerable provided $a_s \gtrsim a_f$

or equivalently that $\beta_s \lesssim \beta_f$. For the $3+1d$ Wilson action, β_f are known. In the case of $U(1)$ where $\beta_s = 1$, $\mathbb{Z}_{n>5}$ satisfies $\beta_f > \beta_s$. For nonabelian gauge groups, only a few crystal-like subgroups exist. $SU(2)$ has three: the binary tetrahedral $\mathbb{BT}$, the binary octahedral $\mathbb{BO}$, and the binary icosahedral $\mathbb{BI}$. The scaling regime for $SU(2)$ occurs around $\beta_s = 2.2$. Therefore, a value of $\beta_f = 2.24(8)$ for $\mathbb{BT}$ is unlikely to prove useful with just the Kogut-Susskind Hamiltonian H_{KS}, although experience with $SU(3)$ suggests modified or improved Hamiltonians H_I would prove sufficient [32, 56, 78, 79]. The other two groups, $\mathbb{BO}$ and $\mathbb{BI}$, have values far into the scaling regime: $\beta_f = 3.26(8)$ and $\beta_f = 5.82(8)$, respectively [32].

Substantial work has studied the quantum simulation of abelian theories, particularly in low dimensions. Despite this, one must remember that nonabelian gauge theories demonstrate many behaviors unseen in abelian ones; thus, results for $U(1)$ or $\mathbb{Z}_N$ may fail to represent the full complexity of lattice gauge theories. The group of interest in this paper, the 24-element $\mathbb{BT}$, is the smallest crystal-like subgroup of a nonabelian theory and requires 5 qubits per register. The dihedral groups, D_N, while not crystal-like, have previously been investigated for simulation on quantum computers [7, 19, 20, 88]. Having $2N$ elements respectively, they require $\lceil \log_2(2N) \rceil$ qubits per register. Further studies have been undertaken to understand the $\mathbb{Q}_8$ subgroup of $SU(2)$ [72] which requires only 3 qubits.

In the interest of studying quantum simulations on near-term devices, we should consider both $3 + 1d$ and $2 + 1d$ theories. Using classical lattice simulations, we have determined that in both spacetimes $\beta_f \approx \beta_s$ for the Wilson action (See Fig. 1). Thus quantum simulations with $\mathbb{BT}$ require an improved Hamiltonian [21] and will be the only one considered in this work. Since $a_f \propto e^{-\beta_f}$ within the scaling regime, only a small improvement in the Hamiltonian is needed.

In this paper, we construct quantum circuits implementing the four primitive gates (inversion, multiplication, trace, and Fourier) required to simulate the $\mathbb{BT}$ theories. We will consider two possible quantum devices when constructing our gates. The first is a qubit-based device. The second device, motivated by the potential for bosonic quantum comptuers [89], is a $d = 24$ qudit device where
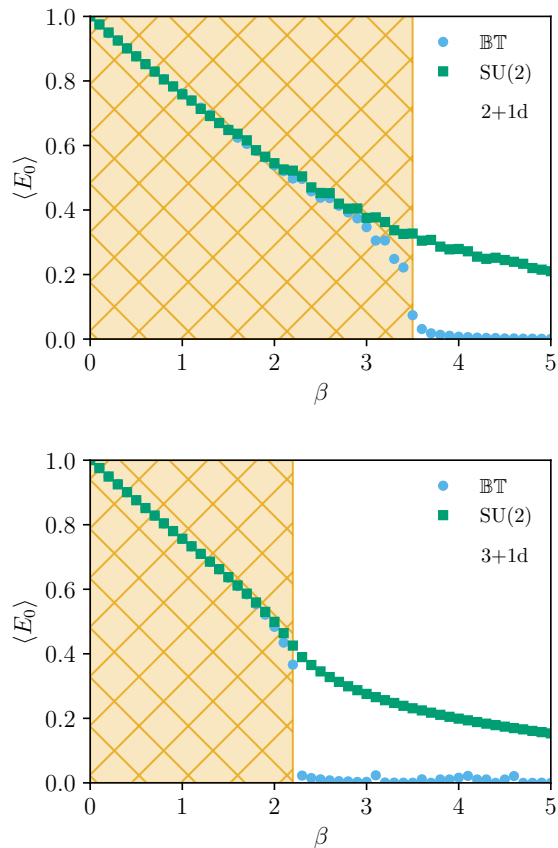
FIG. 1. Euclidean calculations of lattice energy density $\langle E_0 \rangle$ of $\mathbb{BT}$ as measured by the expectation value of the plaquette as a function of Wilson coupling β on 4^d lattices for (top) $2+1d$ (bottom) $3+1d$. The shaded region indicates $\beta \leq \beta_s$.

only one qudit is required per register. We refer to this d=24 state qudit as a *quicosotetrit*. Although time evolution on quantum processors is infeasible at present due to the low gate fidelities and coherence time, we benchmark the process fidelity of the inversion and trace gates for $\mathbb{BT}$ on the `ibm_nairobi` QPU to evaluate the improvements needed for simulations on quantum processors.

This paper is organized as follows. In Sec. II, the necessary group theoretic properties of $\mathbb{BT}$ are summarized and the digitization scheme is presented. A review of the basic qubit and qudit gates used in this work is found in Sec. III. Sec. IV summarized the four primitive gates required for implementing the group operations. This is followed by quantum circuit constructions for these gates for $\mathbb{BT}$ gauge theories: the inversion gate in Sec. V, the multiplication gate in Sec. VI, the trace gate in Sec. VII, and the Fourier transform gate in Sec. VIII. Benchmark results for our $\mathbb{BT}$ inversion and trace gates are found in Sec. IX. Using these gates, Sec. X presents a resource estimates for simulating $3 + 1d$ $SU(2)$. We conclude and discuss future work in Sec. XI.

II. PROPERTIES OF $\mathbb{BT}$

The simulation of lattice gauge theories requires the definition of a register where one can store the state of a bosonic link variable which we call a $G-$register. In order to construct the $\mathbb{BT}-$register in term of integers, it is necessary to construct a mapping between the 24 elements of the group and the integers $[0, 23]$. A clean way to obtain this is to write every element of $\mathbb{BT}$ as an ordered product of four generators[1] with exponents written in terms of the binary variables m, n, o, p, q:

$$g = (-1)^m \mathbf{i}^n \mathbf{j}^o \mathbf{l}^{p+2q}, \tag{1}$$

with

$$\mathbf{l} = -\frac{1}{2}(\mathbb{1} + \mathbf{i} + \mathbf{j} + \mathbf{k}) \tag{2}$$

and $\mathbf{i}$, $\mathbf{j}$, $\mathbf{k}$ are the unit quaternions which in the 2d irreducible representation (irrep) correspond to Pauli matrices. With the construction of Eq. (1), the $\mathbb{BT}-$register is given by a binary encoding of the qubits with the ordering $|qponm\rangle$. While there exist 2^5 possible state in a 5 qubit register, we only consider the 24 lowest state represent group elements. The states $|24\rangle$ thru $|31\rangle$ are unphysical. This is equivalent to never considering cases where $p = q = 1$. In this work we will use a short hand $|N\rangle$ to correspond to a given bit string $|qponm\rangle$ where the number N is the integer representation of the binary string $qponm$ with most significant bit first. This same mapping can be utilized for quicosotetrits . For example, using $\eta = 1 + i$ one element in the real 2d irrep is

$$\frac{1}{2}\begin{pmatrix} \eta & \eta^* \\ -\eta & \eta^* \end{pmatrix} = (-1)^1 \mathbf{i}^1 \mathbf{j}^1 \mathbf{l}^{0+2\times 1} \rightarrow |10111\rangle = |23\rangle \tag{3}$$

The $\mathbf{i}$, $\mathbf{j}$, and $\mathbf{k}$ generators anti-commute with each other. Additional useful relations are:

$$\begin{aligned} &\mathbf{i}^2 = \mathbf{j}^2 = -\mathbb{1}, \ \mathbf{l}^3 = \mathbb{1} \\ &\mathbf{ij} = \mathbf{k}, \ \mathbf{jk} = \mathbf{i}, \ \mathbf{ki} = \mathbf{j}, \\ &\mathbf{li} = \mathbf{jl}, \ \mathbf{lj} = \mathbf{kl}, \ \mathbf{lk} = \mathbf{il}, \\ &\mathbf{l}^2\mathbf{i} = \mathbf{kl}^2, \ \mathbf{l}^2\mathbf{j} = \mathbf{kl}^2, \ \mathbf{l}^2\mathbf{k} = \mathbf{jl}^2. \end{aligned} \tag{4}$$

The character table (Table I) lists important group properties; the different irreps can be identified by the value of their character acting on each element. An irrep's dimension is the value of the character of $\mathbb{1}$. There are three $1d$ irreps, three $2d$ irreps (one real and two complex), and one $3d$ irrep. To derive the Fourier transform, it is

---

[1] The minimal set of generators for $\mathbb{BT}$ is two, but we have been unable to find an ordered product with less than three. The choice of three generators is the same as the one with four generators where $(-1)^m \mathbf{i}^n \rightarrow \mathbf{i}^{2m+n}$. Nevertheless the qubit costs cannot go below the current formulation's value of $\lceil \log_2(24) \rceil = 5$.

necessary to know a matrix presentation of each irrep. Based on our qubit mapping, given a presentation of $-1, \mathbf{i}, \mathbf{j}$, and $\mathbf{l}$ we can construct any element of the group from Eq. (1). With the 3rd root of unity $\omega = e^{2\pi i/3}$, the 1d irreps are given:

$$\rho_1 : -1 = \mathbf{i} = \mathbf{j} = \mathbf{l} = 1 \tag{5}$$

$$\rho_2 : -1 = \mathbf{i} = \mathbf{j} = 1, \; \mathbf{l} = \omega^2 \tag{6}$$

$$\rho_3 : -1 = \mathbf{i} = \mathbf{j} = 1, \; \mathbf{l} = \omega \tag{7}$$

Now for the 2d irreps, we can use for all three irreps the same definitions:

$$\rho_{4,5,6} : -1 = \text{diag}(-1,-1), \; \mathbf{i} = \text{diag}(i,-i),$$
$$\mathbf{j} = \begin{pmatrix} 0 & -1 \\ 1 & 0 \end{pmatrix}, \; \mathbf{l} = -\frac{1}{2} \begin{pmatrix} \eta & -\eta \\ \eta^* & \eta^* \end{pmatrix} \tag{8}$$

then we can construct the three 2d irreps by taking:

$$\rho_4(g) = (-1)^m \mathbf{i}^n \mathbf{j}^o \mathbf{l}^{p+2q} \tag{9}$$

$$\rho_5(g) = (-1)^m \mathbf{i}^n \mathbf{j}^o (\omega^2 \mathbf{l})^{p+2q} \tag{10}$$

$$\rho_6(g) = (-1)^m \mathbf{i}^n \mathbf{j}^o (\omega \mathbf{l})^{p+2q} \tag{11}$$

For the 3d irrep, we have

$$\rho_7 : -1 = \text{diag}(1,1,1), \quad \mathbf{i} = \text{diag}(-1,1,-1),$$
$$\mathbf{j} = \text{diag}(1,-1,-1), \quad \mathbf{l} = \begin{pmatrix} 0 & 1 & 0 \\ 0 & 0 & 1 \\ 1 & 0 & 0 \end{pmatrix} \tag{12}$$

TABLE I. Character Table of $\mathbb{BT}$ including an enumeration of the elements in the given class.

Size	1	1	6	4	4	4	4
Order	1	2	4	6	6	3	3
ρ_1	1	1	1	1	1	1	1
ρ_2	1	1	1	ω	ω^2	ω^2	ω
ρ_3	1	1	1	ω^2	ω	ω	ω^2
ρ_4	2	-2	0	1	1	-1	-1
ρ_5	2	-2	0	ω^2	ω	$-\omega^2$	$-\omega$
ρ_6	2	-2	0	ω^2	ω	$-\omega$	$-\omega^2$
ρ_7	3	3	-1	0	0	0	0
$|g\rangle$	$\|0\rangle$	$\|1\rangle$	$\|2\rangle,\|3\rangle$ $\|4\rangle,\|5\rangle$ $\|6\rangle,\|7\rangle$	$\|9\rangle,\|10\rangle$ $\|12\rangle,\|14\rangle$	$\|17\rangle,\|19\rangle$ $\|21\rangle,\|23\rangle$	$\|8\rangle,\|11\rangle$ $\|13\rangle,\|15\rangle$	$\|16\rangle,\|18\rangle$ $\|20\rangle,\|22\rangle$

III. QUBIT AND QUDIT GATES

In order to implement the group primitive gates on qubit and qudit hardware we need a set of quantum gate operations. We begin by first enumerating the qubit gates, followed by a discussion of the qudit gates.

The first basic qubit gates we need are the Pauli gates $p = X, Y, Z$. These can be extended to arbitrary rotations about their respective axes $R_p(\theta) = e^{i\theta p/2}$. When decomposing onto fault-tolerant devices, the $T = \text{diag}(1, e^{i\pi/4})$ gate becomes relevant.

The first multiqubit operation we need is the SWAP operation, which swaps two qubits:

$$\text{SWAP} \; |a\rangle \otimes |b\rangle = |b\rangle \otimes |a\rangle.$$

The controlled not (CNOT) gate applies the X operation on a target qubit if the control qubit is in the state $|1\rangle$:

$$\text{CNOT} \; |a\rangle \otimes |b\rangle = |a\rangle \otimes |b \oplus a\rangle,$$

where $\oplus$ indicates addition modulus 2. We also need the following multiqubit gates: C^nNOT – of which C^2NOT is called the Toffoli gate – and CSWAP (Fredkin) gates. The C^nNOT gate is the further extension to the case of where the n control qubits must be in the $|1\rangle^{\otimes n}$ state. For example, the Toffoli in terms of modular arithmetic is

$$\text{C}^2\text{NOT} \; |a\rangle \otimes |b\rangle \otimes |c\rangle = |a\rangle \otimes |b\rangle \otimes |c \oplus ab\rangle.$$

The CSWAP gate swaps two qubit states if the control is in the $|1\rangle$ state:

$$\text{CSWAP} \; |a\rangle \otimes |b\rangle \otimes |c\rangle = |a\rangle \otimes |b(1 \oplus a) \oplus ac\rangle \\ \otimes |c(1 \oplus a) \oplus ab\rangle.$$

One final qubit operation, the controlled permutation gate $C\chi$, will prove useful to define for conciseness later. Fig. 2 constructs it in terms of C^nNOT gates.
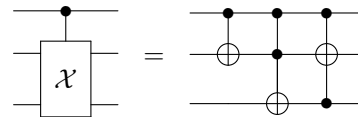

FIG. 2. The controlled permutation gate, $C\chi$.

We also need a set of gates for implementation on quicosotetrit device. In our case, there are not specialized quicosotetrit gates but a general set of qudit ones to consider. The single qudit gates we need are: Givens rotations, the selective number of arbitrary photon (SNAP) [90, 91], displacement [92], and photon blockade gates [93, 94].

Givens rotations $R_p^{(a,b)}(\theta)$ are generalizations of $R_p(\theta)$ to qudits where rotations occur in the subspace of states

$|a\rangle$ and $|b\rangle$ while leaving all the other states untouched. We also use the notation $p^{(a,b)}$ to indicate special Givens rotations that correspond to the generalized Pauli gates (e.g. $X^{(3,4)}$). These gates are useful in designing algorithms for simulating with qudits, but are difficult to natively implement. Therefore real simulations will likely require their decomposition.

One native gate set for single qudits in cavity QED devices is SNAP and displacement gates [90–92]. SNAP gates can arbitrarily phase the qudit states:

$$\mathcal{S}(\vec{\theta}) = \sum_{a=0}^{N-1} |a\rangle \langle a| \, e^{i\theta_a} \qquad (13)$$

where the sum is over computational basis states $a = [0, N-1]$ of an $N-$state qudit and $\vec{\theta} = \{\theta_0, \theta_1, \ldots, \theta_{N-1}\}$ are a set of tunable parameters analogous to θ in $R_Z(\theta)$.

The displacement gate coherently changes the cavity's photon number. In terms of Fock-operators $\hat{a}, \hat{a}^\dagger$, it is

$$\mathcal{D}(\alpha) = e^{\alpha \hat{a}^\dagger - \alpha^* \hat{a}}. \qquad (14)$$

The photon blockade operation acts as an $R_X(\theta)$ or $R_Y(\theta)$ rotation between two Fock states in a cavity by driving the system at an off-resonant frequency while shifting the desired modes to said frequency [93, 94].

In order to obtain a universal set of gates, we require an entangling gate. One proposal is the controlled SNAP gate which phases a target qudit based on if a second qudit is in a state $|\alpha\rangle$ [95]:

$$c\mathcal{S}(\vec{\theta}, \alpha) = \sum_{a=0, a\neq\alpha}^{N-1} |a\rangle\langle a| \otimes \mathbb{1} + |\alpha\rangle\langle\alpha| \otimes \sum_{b=0}^{N-1} |b\rangle\langle b| e^{i\theta_b}. \qquad (15)$$

IV. OVERVIEW OF PRIMITIVE GATES

For general gauge groups, it is possible to define any quantum circuit with sets of primitive gates. Using this formulation confers two benefits: first, it is possible to design algorithms in a theory- and hardware-agnostic way; second, the circuit optimization is split into smaller, more manageable pieces. This construction begins with defining for G a G-register by identifying each group element with a computational basis state $|g\rangle$, where $g \in G$. One choice of primitive gates is: inversion $\mathfrak{U}_{-1}$, multiplication $\mathfrak{U}_\times$, trace $\mathfrak{U}_{\text{Tr}}$, and Fourier transform $\mathfrak{U}_F$ [19].

The inversion gate, $\mathfrak{U}_{-1}$, is a single register gate which takes a group element to its inverse:

$$\mathfrak{U}_{-1} |g\rangle = \left|g^{-1}\right\rangle. \qquad (16)$$

The group multiplication gate acts on two $G-$registers. It takes the target $G-$register and changes the state to the left product with the control $G-$register:

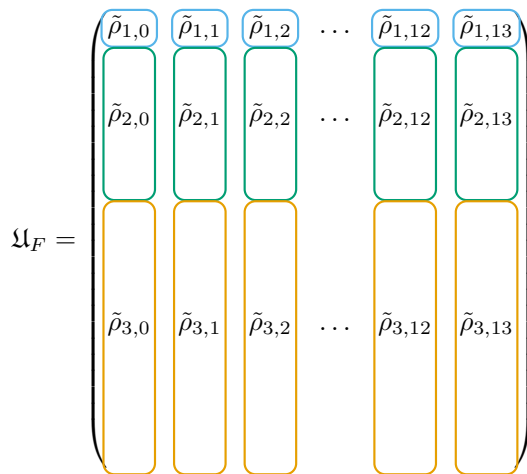$$\mathfrak{U}_\times |g\rangle |h\rangle = |g\rangle |gh\rangle. \qquad (17)$$

FIG. 3. Example $\mathfrak{U}_F$ from Eq. (19) using column vectors $\tilde{\rho}_{i,j} = \sqrt{d_\rho/|G|}\rho_{i,j}$ where $\rho_{i,j} = \rho_i(g_j)$. This example has three irreps with $d_\rho = 1, 2, 3$. $\mathfrak{U}_F$ is square since $\sum_\rho d_\rho^2 = |G|$

Left multiplication is sufficient for a minimal set as right multiplication can be implemented use two applications of $\mathfrak{U}_{-1}$ and $\mathfrak{U}_\times$, albeit optimal algorithms may take advantage of an explicit construction [21].

The trace of products of group elements appears in lattice Hamiltonians. We can implement these terms by combining $\mathfrak{U}_\times$ with a single-register trace gate:

$$\mathfrak{U}_{\text{Tr}}(\theta) |g\rangle = e^{i\theta \, \text{Re Tr } g} |g\rangle. \qquad (18)$$

The final gate required is the group Fourier transform $\mathfrak{U}_F$. The Fourier transform of a finite G is defined as

$$\hat{f}(\rho) = \sqrt{\frac{d_\rho}{|G|}} \sum_{g \in G} f(g)\rho(g), \qquad (19)$$

where $|G|$ is the size of the group, d_ρ is the dimensionality of the representation ρ, and f is a function over G. The inverse transform is given by

$$f(g) = \frac{1}{\sqrt{|G|}} \sum_{\rho \in \hat{G}} \sqrt{d_\rho} \, \text{Tr} \, (\hat{f}(\rho)\rho(g^{-1})), \qquad (20)$$

where the dual $\hat{G}$ is the set of all irreducible representations (irrep) of G. The gate that performs this acts on a single G-register with some amplitudes $f(g)$ which rotate it into the Fourier basis:

$$\mathfrak{U}_F \sum_{g \in G} f(g) |g\rangle = \sum_{\rho \in \hat{G}} \hat{f}(\rho)_{ij} |\rho, i, j\rangle. \qquad (21)$$

The second sum is taken over ρ, the irreducible representations of G; $\hat{f}$ denotes the Fourier transform of f. After application of the gate, the register is denoted as a $\hat{G}$-register to indicate the change of basis. A schematic example of this gate is show in Fig. 3
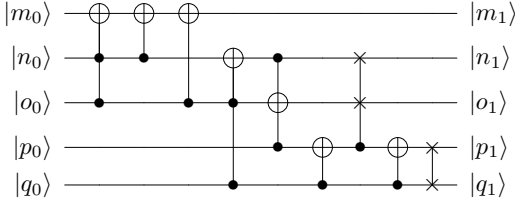
FIG. 4. A qubit implementation of $\mathfrak{U}_{-1}$ which uses Toffoli and CSWAP gates. These multiqubit entangling gates can be decomposed into one- and two-qubit gates as discussed in the literature.

V. INVERSION GATE

Consider a $\mathbb{BT}-$register storing the group element given by $g = (-1)^{m_0}\mathbf{i}^{n_0}\mathbf{j}^{o_0}\mathbf{l}^{p_0+2q_0}$. The effect of the inversion gate on this register is to transform it to

$$|g\rangle = |q_0 p_0 o_0 n_0 m_0\rangle \rightarrow |g^{-1}\rangle = |q_1 p_1 o_1 n_1 m_1\rangle. \quad (22)$$

Using Eq. (1) and $(AB)^{-1} = B^{-1}A^{-1}$, the inverse of g is

$$g^{-1} = (-1)^{m_0+n_0+o_0}\mathbf{l}^{3-p_0-2q_0}\mathbf{j}^{o_0}\mathbf{i}^{n_0}.$$

We can then put this into the normal ordering of Eq. (1) using the relations in Eq. (4) to find:

$$g^{-1} = (-1)^{m_1}\mathbf{i}^{n_1}\mathbf{j}^{o_1}\mathbf{l}^{p_1+2q_1}. \quad (23)$$

where the relation between the $|g\rangle$ and $|g^{-1}\rangle$ indices are :

$$
\begin{aligned}
m_1 &= m_0 + n_0 + o_0 + n_0 \times o_0 \\
n_1 &= n_0(1 - q_0) + o_0(p_0 + q_0) \\
o_1 &= o_0(1 - p_0) + n_0(p_0 + q_0) \\
p_1 &= q_0 \\
q_1 &= p_0.
\end{aligned}
\quad (24)
$$

A qubit circuit implementation of $\mathfrak{U}_{-1}$ is shown in Fig. 4. We can map Eq. (24) onto a quantum circuit using modular arithmetic, finding that transforming m_0 to m_1 uses two CNOTs and a Toffoli gate. A circuit with a CSWAP and two Toffolis is required for n_1 and o_1, while p_1 and q_1 need one SWAP.

The quicosotetrit circuit of $\mathfrak{U}_{-1}$ is simpler, needing only 11 $X^{(a,b)}$ gates[2], as seen in Fig. 5. 24 $\mathcal{S}(\vec{\theta})$ and 25 $\mathcal{D}(\alpha)$ are sufficient to approximate $\mathfrak{U}_{-1}$ to sub-percent infidelity. Inspecting this circuit, the largest separation between inverses is $|10\rangle$ and $|23\rangle$. Using only $\mathcal{S}(\vec{\theta})$ and $\mathcal{D}(\alpha)$, this could prove noisy in terms of the necessary $\vec{\theta}$ and α, and thus large-separation photon blockade gates are desirable.

---

[2] $1 X^{(a,b)}$ of the 12 is unnecessary since $|0^{-1}\rangle = |0\rangle$ and $|1^{-1}\rangle = |1\rangle$

VI. MULTIPLICATION GATE

The method to construct the $\mathfrak{U}_{\times}$ for qubits is similar to that for $\mathfrak{U}_{-1}$. Given two $\mathbb{BT}-$registers storing g and h:

$$g = (-1)^{m_0}\mathbf{i}^{n_0}\mathbf{j}^{o_0}\mathbf{l}^{q_0+2p_0}, \ h = (-1)^{m_1}\mathbf{i}^{n_1}\mathbf{j}^{o_1}\mathbf{l}^{q_1+2p_1}, \quad (25)$$

we want $gh = g \times h$ and permuting $|h\rangle$ to $|gh\rangle$. Defining $gh = (-1)^{m_2}i^{n_2}j^{o_2}l^{2p_2+q_2}$, we can derive via Eq. (4):

$$
\begin{aligned}
m_2 &= o_1 n_0(1 - p_1) + (n_1 n_0 + o_1 o_0)(1 - q_1) \\
&\quad + n_1 o_0(p_1 + q_1) \\
n_2 &= n_1 + n_0(1 - q_1) + o_0(p_1 + q_1) \\
o_2 &= o_1 + o_0(1 - p_1) + n_0(p_1 + q_1) \\
p_2 &= p_0(1 - q_1)(1 - p_1) \\
q_2 &= q_0(1 - q_1)(1 - p_1).
\end{aligned}
\quad (26)
$$

These expressions map into the qubit circuit of Fig. 6.

$\mathcal{U}_{\times}$ on quicosotetrits is a permutation of $|h\rangle$ controlled by $|g\rangle$ realized as

$$\mathcal{U}_{\times} = \sum_{g \in G}\sum_{h \in G}|g\rangle\langle g| \otimes |h\rangle\langle g \times h| = \sum_{g \in G}|g\rangle\langle g| \otimes \hat{P}_g,$$

where $\hat{P}_g$ is a permutation matrix that depends upon g. This unitary matrix can be diagonalized by one-qudit gates V_g. A quicosotetrit circuit for $\mathfrak{U}_{\times}$ is shown in Fig. 8.

The structure of V_g depends on the order m of the element g (Tab. I) being multiplied onto the element h. For a given operator g the elements $h \in G$ will break down into $24/m$ sets of m elements. The elements in each set are determined solely by the operator g itself. The elements in each set can be generated by taking h and left multiplying it by g until the element h is reached again. These sets of elements will provide a presentation of a $\mathbb{Z}_m$ group. In this way V_g can be rendered into a set of $24/m$ blocks of size m. These blocked sections with at most an $SU(6)$ rotation in the given subspace. The $SU(N)$ Euler angle decompositions are provided in Appendix A along with the group cycles generated by each g. Tab. II provides the total number of $R_p^{(a,b)}(\theta)$ for each $QFT_{\mathbb{Z}_m}$ on the m-level subspace as well as V_g.

A directed graph for the group sets for $g = -1$, $\mathbf{l}$, and $-\mathbf{l}$ ($|1\rangle$, $|8\rangle$, $|9\rangle$ respectively) are shown in Fig. 7. In this figure we show how multiplication of a group element h on the left by a group element g will cycle through a subset of the group elements in a directed graph. For example multiplication by -1 ($|1\rangle$) flip flops elements $|2a\rangle$ and $|2a+1\rangle$. In this way the neighboring states will have a $\mathbb{Z}_2$ Fourier transform applied on each pair. Multiplication by the element $\mathbf{l}$ ($|8\rangle$) will cycle the states $|a\rangle$, $|a+8\rangle$, and $|a+16\rangle$ for $a \leq 7$. The cycles shown for multiplication by $-\mathbf{l}$ ($|9\rangle$), are more complicated to write in closed form but are shown in the right hand side of Fig. 7.

In this way $V_g^{\dagger}\hat{P}_g V_g$ will be a diagonal matrix whose nonzero elements are phases corresponding to the eigenvalues of $\hat{P}_g$. As we iterate through g_i, neighboring $V_{g_i}V_{g_{i+1}}^{\dagger}$
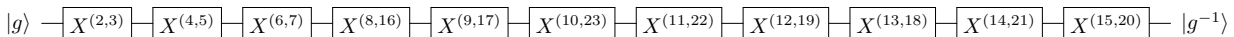
FIG. 5. A quicosotetrit implementation of $\mathfrak{U}_{-1}$ using the $X^{(a,b)}$ gate. States $|0\rangle$ and $|1\rangle$ are unaffected because they are their own inverse.
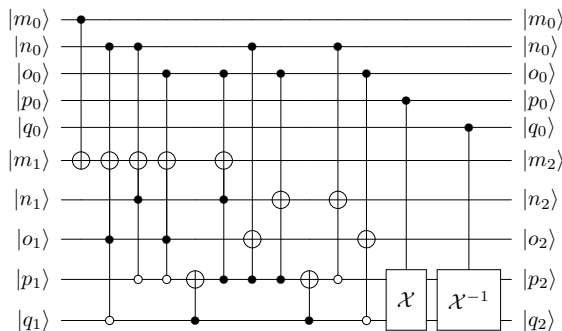

FIG. 6. A qubit implementation of $\mathfrak{U}_\times$. Following convention, filled (open) circles correspond to control on $|1\rangle$ ($|0\rangle$). The Cχ gate is defined in Fig. 2 and Cχ^{-1} is its inverse.

TABLE II. $R_p^{(a,b)}(\theta)$ required for $QFT_{\mathbb{Z}_m}$ and V_g for each order. $N_{|g\rangle}$ denote the number of elements with that cycle.

cycle	$N_{|g\rangle}$	$R_p^{(a,b)}(\theta)$ in $QFT_{\mathbb{Z}_m}$	$R_p^{(a,b)}(\theta)$ in V_g
1	1	0	0
2	1	3	36
3	8	8	64
4	6	15	90
6	8	35	140

can be combine into a single qudit operation. If we use Tab. II as a starting point and recognize that for the order 3, 4, and 6 that V_g's appear in pairs of states, almost half of the $R_p^{(a,b)}(\theta)$ are eliminated, leaving 2,244 to implement all V_g's. In terms of native gates, $\mathfrak{U}_\times$ needs 575 SNAP and 575 $\mathcal{D}(\alpha)$ gates in addition to the 23 cSNAP gates for $\hat{P}_g$. This cost could be reduced by pulse engineering, an active research area in bosonic quantum computers [96–99].
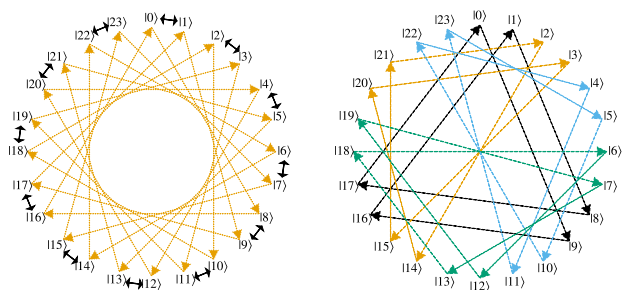

FIG. 7. Left: Pictorial representation of the cycles for $|g\rangle$ being: $|1\rangle$ with $m = 2$, (black arrows); $|8\rangle$ with $m = 3$, (orange dotted arrows). Right: representation of the cycle for $|9\rangle$ with $m = 6$, different cycles are shown in different colors.

VII. TRACE GATE

For simulating gauge theories, $\mathfrak{U}_{\text{Tr}}$ is only needed for the fundamental representation, ρ_4. The character table (Tab. I) provides us with the $\text{Re Tr}(g_i)$ necessary. $\mathfrak{U}_{\text{Tr}}$ can be obtained by defining a Hamiltonian, and then exponentiating it. For our qubit-register, H_{tr} for ρ_4 is

$$H_{\text{Tr}} = Z_{m_0}\Big(Z_{q_0}\big[2 + \big(1 + Z_{o_0}\big)\big(Z_{n_0} + Z_{p_0}(1 + Z_{n_0})\big)\big]$$
$$+ Z_{p_0}\big[Z_{o_0} + Z_{n_0} - 1\big]\Big)$$

(27)

were Z_h acts on the $|h\rangle$ qubit. From this, we can decomposing $e^{i\theta H_{tr}}$ into the linear combinations of $R_Z(\theta)$ gates. The qubit-based circuit for $\mathfrak{U}_{\text{Tr}}$ is shown in Fig. 9.

Implementing $\mathfrak{U}_{\text{Tr}}$ on a quicosotetrit requires 9 $R_Z^{(a,b)}(\theta)$ gates corresponding to the 9 $(g_i, -g_i)$ pairs with $\text{Re Tr}(g_i) \neq 0$; this gate is shown in Fig. 10. Together, these gates can be mapped to a single SNAP gate.

VIII. FOURIER TRANSFORM

The standard n-qubit quantum Fourier transform (QFT) [100] corresponds to the quantum version of the fast Fourier transform of $\mathbb{Z}_{2^n}$. Quantum Fourier transforms over several nonabelian groups exist in the literature [20, 101–104]. Alas, for all the crystal-like subgroups of interest to high energy physics efficient QFT circuits are currently unknown [105]. For the general case, there isn't a clear algorithmic way to construct the QFT. Therefore, we instead construct a suboptimal $\mathfrak{U}_F$ from Eq. (19) using the irreps of Sec. II to obtain the matrix in Fig. 11. The structure of the Fourier transform is ordered as follows. The columns index group elements $|g\rangle$ from $|0\rangle$ to $|24\rangle$ according to Eq. (1). We then index the irreducible representation ρ_i ordered sequentially from $i = 1$ to $i = 7$. For each ρ_i, we convert the $d_{\rho_i}^2$ matrix representation of g into a column vector. For example, the first three rows of Fig. 11 correspond to the 1d irreps ρ_1, ρ_2, and ρ_3. Then rows 4 through 7 are the matrix elements of the $d_4 = 2$ ρ_4 as a column vector.

Since $\mathbb{BT}$ has 24 elements, on a qubit device $\mathfrak{U}_F$ must be embedded into a larger $2^d \times 2^d$ matrix. With this matrix, a transpiler can be used to derive a circuit. Using the QISKIT transpiler, $\mathfrak{U}_F$ requires 1025 CNOTs, 2139 $R_Z(\theta)$, and 1109 $R_Y(\theta)$; the Fourier gate is the most expensive qubit primitive. As will be discussed in Sec. X, $\mathfrak{U}_F$ dominates the total simulation costs and future work should be devoted to finding a $\mathbb{BT}$ QFT.
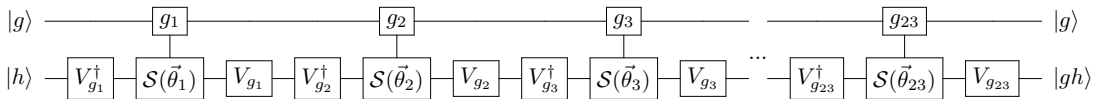
FIG. 8. A quicosotetrit implementation of $\mathfrak{U}_\times$. The subscript g_i indicates the the ith element of the group.
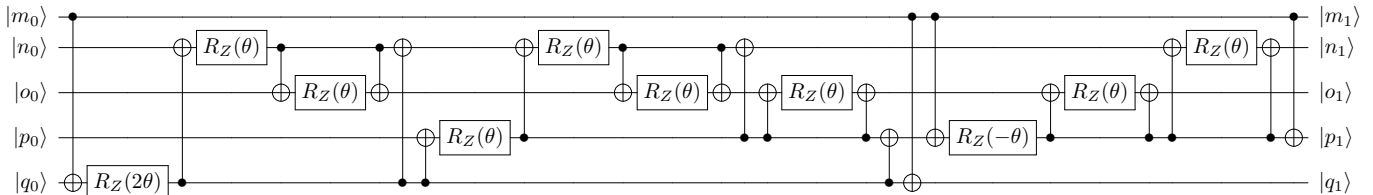

FIG. 9. A qubit implementation of $\mathfrak{U}_{\mathrm{Tr}}$.

A quicosotetrit implementation follows the same generalized Euler angle decomposition as the V_g used for $\mathfrak{U}_\times$ [106]. This gate can be implemented with 24 SNAP and 25 displacement gates to subpercent infidelity.

IX. EXPERIMENTAL RESULTS

In this section, we discuss experimental results from running $\mathfrak{U}_{-1}$ and $\mathfrak{U}_{\mathrm{Tr}}$ on the `ibm_nairobi` 7 transmon qubit device (see Fig. 12). Transpiling Fig. 4 and Fig. 9 onto `ibm_nairobi`, topology constraints require introducing additional SWAP gates (see Fig. 12). The cost of $\mathfrak{U}_{\mathrm{Tr}}$ increases from 22 CNOTs to 39, and for $\mathfrak{U}_{-1}$ the number of CNOTs goes from 31 to 49. The high qubit cost of $\mathfrak{U}_\times$ and high gate costs of $\mathfrak{U}_F$ suggest they are unlikely to have reasonable fidelities and they are left for the future.

We define the process fidelity $\mathcal{F}$ of $\mathfrak{U}$ on a state $|\psi\rangle$ as

$$\mathcal{F}_{\mathfrak{U}}^{|\Psi\rangle} = |\langle 0|\Psi^\dagger \mathfrak{U}^\dagger \mathfrak{U}\Psi|0\rangle|^2 \tag{28}$$

Without noise, the state preparation Ψ and $\mathfrak{U}$ are exactly cancelled by their complex conjugations, thus the measured result should always be $|0\rangle^{\otimes 5}$. Determining the fidelity requires testing all the possible states $|\Psi\rangle$, a prohibitively expensive task [107]. Therefore we consider a subset of states given by the 24 group element states $|g\rangle$ which can be obtained by applying X gates to the appropriate qubits. For a general state, $\Psi^\dagger \mathfrak{U}^\dagger$ could require as many CNOTs as $\mathfrak{U}\Psi$. In this case, the total circuit cost is doubled and fidelities are reduced. In contrast, for $|g\rangle$, the results of applying either of our gates is another $|g\rangle$, which can be returned to $|0\rangle^{\otimes 5}$ using only X gates. With this, we compute $\mathcal{F}$ for each $|g\rangle$ for both $\mathfrak{U}_{\mathrm{Tr}}$ and $\mathfrak{U}_{-1}$ without doubling the CNOT count. With these results we calculate a mean value $\bar{\mathcal{F}}_{\mathfrak{U}}$.

The dominant coherent CNOT error can be mitigated through Pauli twirling [108–112]. This method converts coherent errors into random Pauli channel errors and has found success in lattice applications [21, 113]. The circuits are modified by wrapping each CNOT with a set of Pauli gates $\{\mathbb{1}, X, Y, Z\}$ sampled from sets which are logical equivalent to CNOT. We ran 20 unique circuits for each gate-state pair following prior results finding $\mathcal{O}(10)$ circuits to suffice [108]. 2000 shots were taken for the $\mathfrak{U}_{\mathrm{Tr}}$ circuits, while 500 were gotten for $\mathfrak{U}_{-1}$. The process fidelity for each $|g\rangle$ are shown in Fig. 13. Averaging we find that the $\bar{\mathcal{F}}_{\mathrm{Tr}}^{|g\rangle} = 55(1)\%$, while the higher CNOT count of $\mathfrak{U}_{-1}$ leads to a lower fidelity of $\bar{\mathcal{F}}_{-1}^{|g\rangle} = 37.0(8)\%$.

While $|g\rangle$ are easy to implement, they are less likely to be encountered during a simulations, since states must be gauge invariant. In the case of $\mathfrak{U}_{-1}$, it is possible to test a gauge invariant state $|GI\rangle = |G|^{-1/2} \sum_g |g\rangle$ because both $|GI\rangle$ and $\Psi^\dagger \mathfrak{U}_{-1}^\dagger$ can be implemented with only 1 additional CNOT. For this state, we found a reduced fidelity $\mathcal{F}_{-1}^{|GI\rangle} = 14.8(12)\%$.

X. RESOURCE ESTIMATES

Clearly time evolution for large lattices of $\mathbb{BT}$ is beyond the NISQ era and we should consider fault-tolerant quantum computers. The Eastin-Knill theorem restricts quantum error correcting codes by preventing universal sets of gates from being implemented transversally [114]. Transversality refers to the property that gates operating on logical qubits correspond to tensor products on the physical qubits. For many error correcting codes such as Calderbank-Shor-Steane (CSS) codes the Clifford gates are transversal [107, 115–118] while the T gate is not. Therefore, T gates are an important metric in fault-tolerant algorithm analysis because they require entanglement between physical qubits [107, 119].

The Toffoli gate is known to require 7 T gates [107] and the C^{n}NOT gates can be constructed exactly using a ladder of Toffoli gates and clean ancilla qubits[3] which can be reused later [107, 120]. Using this ladder method

―――――

[3] A *clean* ancilla is a qubit initialized to $|0\rangle$. *Dirty* ancilla indicate ones in an unknown initial state.

$$|g\rangle - \boxed{R_Z^{(0,1)}(2\theta)} - \boxed{R_Z^{(8,9)}(-\theta)} - \boxed{R_Z^{(10,11)}(\theta)} - \boxed{R_Z^{(12,13)}(\theta)} - \boxed{R_Z^{(14,15)}(\theta)} - \boxed{R_Z^{(16,17)}(-\theta)} - \boxed{R_Z^{(18,19)}(-\theta)} - \boxed{R_Z^{(20,21)}(-\theta)} - \boxed{R_Z^{(22,23)}(-\theta)} - |h\rangle$$

FIG. 10. A quicosotetrit implementation of $\mathfrak{U}_{Tr}$ using two level $R_Z^{(a,b)}(\theta)$ gates.

$\mathcal{U}_F =$

FIG. 11. Matrix representation of $\mathfrak{U}_F$ where $\eta = 1 + i$ and $\omega = e^{\frac{2\pi i}{3}}$. The irreducible representations are ordered ρ_1 to ρ_7. The 2d and 3d irreps are then indexed by each element in a row of the matrix through all the rows.

FIG. 12. An example mapping of $|g\rangle = |qponm\rangle$ onto the 7 transmon qubit `ibm_nairobi`. $|q_s\rangle$ correspond to spectator qubits that do no play an active role in computations.

FIG. 13. Process Fidelities, $\mathcal{F}$, for the trace and inverse gate on IBM's computer. The angle used was $\theta = 0.7$. The averages are shown as a shaded band.

a C^nNOT gate can be implemented using $4(n-1)$ Toffoli gates and $n-1$ clean ancilla qubits. Methods exist using dirty ancilla at the cost of more T gates [120, 121]. We arrive at the cost for the R_z gates via [122] where these gates can be approximated to precision ϵ with at worst $1.15 \log(1/\epsilon)$ T gates using the repeat-until-success method. Using these, we can construct fault-tolerant gate cost estimates for $\mathbb{BT}$ (See Tab. III).

TABLE III. Number of physical T gates and clean ancilla required to implement logical gates for (top) basic gates taken from [107] (bottom) primitive gates for $\mathbb{BT}$.

Gate	T gates	Clean ancilla
C^2NOT	7	0
C^3NOT	28	1
CSWAP	7	0
R_z	$1.15 \log_2(1/\epsilon)$	0
$\mathcal{U}_{-1}$	28	0
$\mathcal{U}_\times$	154	1
$\mathcal{U}_{Tr}$	$12.65 \log_2(1/\epsilon)$	0
$\mathcal{U}_{FT}$	$1150 \log_2(1/\epsilon)$	0

TABLE IV. Number of primitive gates per link per δt neglecting boundary effects as a function of dimension d for H_I.

Gate	$N[H_I]$
$\mathfrak{U}_F$	4
$\mathfrak{U}_{Tr}$	$\frac{3}{2}(d-1)$
$\mathfrak{U}_{-1}$	$2 + 11(d-1)$
$\mathfrak{U}_\times$	$4 + 26(d-1)$

Primitive gate costs for implementing the improved Hamiltonian, H_I, per link per Trotter step δt are shown in Tab. IV. Using these costs we find that a d spatial lattice simulation of H_I for time $t = N_t \delta t$ would require

$$N_T = \left[4312d - 3640 + \left(4581.03 + 18.975d \log_2 \frac{1}{\epsilon}\right) \right] dL^d N_t \tag{29}$$

Following [123, 124], we consider a fiducial simulation of the shear viscosity η on a $d = 3$ lattice of $L = 10$ with $N_t = 50$, $\epsilon = 10^{-8}$ and the cost of state preparation neglected. For an $SU(2)$ simulation including fermions, Kan and Nam estimated 3×10^{34} T gates, while neglecting fermions allows for a more modest 3×10^{19}. Here, we neglect fermions and using $\mathbb{BT}$ to approximate $SU(2)$ requires 2.0×10^{10} T gates for H_I. So using $\mathbb{BT}$ reduces the gate costs by 9 orders of magnitude. The T gate density is 1 T gate per $\mathbb{BT}$−register per clock cycle and is independent of primitive, although a QFT might increase this. The large reduction in T gates compared to [124] comes by avoiding quantum fixed-point arithmetic. For us, $\mathfrak{U}_F$ dominates the simulations – 44% of the total cost.

Compared to qubits, the field of quantum error correction for qudits is less developed [125–139]. Much, but not all, of the work has focused on qutrits and relies upon specific hardware and native gates. While this field will develop rapidly in the coming years, we will restrict ourselves to quicosotetrit resources estimates based on a device with native cSNAP, SNAP, and displacement gates. The costs for each $\mathbb{BT}$ gate are shown in Tab. V. In contrast to the qubits, for quicosotetrit simulations the most costly gate is $\mathfrak{U}_\times$ with all other gates contributing negligible amounts. Thus, determination of the QFT is

TABLE V. $c\mathcal{S}(\vec{\theta})$, $\mathcal{S}(\vec{\theta})$, and $\mathcal{D}(\alpha)$ gates required for $\mathbb{BT}$ (top) primitive gates (bottom) H_I simulations per link per δt.

Gate	$c\mathcal{S}(\vec{\theta})$	$\mathcal{S}(\vec{\theta})$	$\mathcal{D}(\alpha)$
$\mathcal{U}_{-1}$	0	24	25
$\mathcal{U}_\times$	23	575	575
$\mathcal{U}_{Tr}$	0	1	0
$\mathcal{U}_{FT}$	0	24	25
$e^{-iH_I\delta t}$	$598d - 506$	$15215.5d - 12771.5$	$15225d - 12775$

less important for quicosotetrit devices. Summing the gates, we find the fiducial calculation of the viscosity with 3×10^3 quicosotetrits would require 1.9×10^8 cSNAP and 4.9×10^9 SNAP and displacement gates.

XI. CONCLUSIONS

In this paper, we constructed the necessary primitive quantum circuits for the simulation of $\mathbb{BT}$ – the smallest crystal-like subgroup of $SU(2)$ – gauge theories. These circuits were constructed for both qubit and quicosotetrit architectures and quantum resource estimates were made for the simulation of pure $SU(2)$ shear viscosity. Compared to previous fault-tolerant qubit estimates, we require 10^9 fewer T gates by avoiding quantum fixed point arithmetic via the discrete group approximation. While these simulations are still far off, we performed quantum fidelity experiments for two of the gates. Experimentally, we found the fidelity of the inversion and trace operation to be 37.0(8)% and 55(1)% for classical bit string states on the `ibm_nairobi` quantum processor.

Qudit-based quantum computers, like the quicosotetrit device considered here, are known to require fewer gates, in particular entangling ones. Here we have demonstrated an additional benefit that the construction of nonabelian group primitives are dramatically simplified compared to the qubit case by reducing the complex internal G−register logic required to preserve group structure.

Looking forward, primitive gates should be constructed for larger crystal-like subgroups of $SU(2)$ and to the subgroups of $SU(3)$ theories. At the cost of more qubits and larger lattice errors, a larger $SU(2)$ subgroup should allow the possibility of using the Kogut-Susskind Hamiltonian. This would reduce gate costs by a factor of 2 on a qubit device and a factor of 4 on a qudit one since different primitives dominate the cost. Finally, in order to further reduce the qubit-based simulation gate costs for all discrete subgroup approximations, the formalism for deriving the quantum Fourier transform for each crystal-like subgroup would be of great interest.

ACKNOWLEDGMENTS

[1] R. P. Feynman, Simulating physics with computers, Int. J. Theor. Phys. **21**, 467 (1982).

[2] S. Lloyd, Universal quantum simulators, Science **273**, 1073 (1996).

[3] S. P. Jordan, K. S. M. Lee, and J. Preskill, Quantum Algorithms for Quantum Field Theories, Science **336**, 1130 (2012), arXiv:1111.3633 [quant-ph].

[4] S. P. Jordan, H. Krovi, K. S. Lee, and J. Preskill, BQP-completeness of Scattering in Scalar Quantum Field Theory, Quantum **2**, 44 (2018), arXiv:1703.00454 [quant-ph].

[5] N. Klco, A. Roggero, and M. J. Savage, Standard model physics and the digital quantum revolution: Thoughts about the interface, arXiv preprint arXiv:2107.04769 (2021).

[6] C. W. Bauer *et al.*, Quantum Simulation for High Energy Physics (2022), arXiv:2204.03381 [quant-ph].

[7] J. Bender, E. Zohar, A. Farace, and J. I. Cirac, Digital quantum simulation of lattice gauge theories in three spatial dimensions, New J. Phys. **20**, 093001 (2018), arXiv:1804.02082 [quant-ph].

[8] J. Haah, M. B. Hastings, R. Kothari, and G. H. Low, Quantum algorithm for simulating real time evolution of lattice Hamiltonians (2018).

[9] W. Du, J. P. Vary, X. Zhao, and W. Zuo, Quantum Simulation of Nuclear Inelastic Scattering (2020), arXiv:2006.01369 [nucl-th].

[10] A. M. Childs, Y. Su, M. C. Tran, N. Wiebe, and S. Zhu, Theory of Trotter error with commutator scaling, Phys. Rev. X **11**, 011020 (2021).

[11] E. Campbell, Random compiler for fast Hamiltonian simulation, Phys. Rev. Lett. **123**, 070503 (2019).

[12] D. W. Berry and A. M. Childs, Black-box Hamiltonian simulation and unitary implementation, Quantum Information & Computation **12** (2012).

[13] D. W. Berry, A. M. Childs, R. Cleve, R. Kothari, and R. D. Somma, Simulating Hamiltonian dynamics with a truncated Taylor series, Phys. Rev. Lett. **114**, 090502 (2015).

[14] G. H. Low and I. L. Chuang, Hamiltonian Simulation by Qubitization, Quantum **3**, 163 (2019).

[15] G. H. Low and I. L. Chuang, Optimal Hamiltonian simulation by quantum signal processing, Phys. Rev. Lett. **118**, 010501 (2017).

[16] C. Cirstoiu, Z. Holmes, J. Iosue, L. Cincio, P. J. Coles, and A. Sornborger, Variational fast forwarding for quantum simulation beyond the coherence time, npj Quantum Information **6**, 1 (2020).

[17] J. Gibbs, K. Gili, Z. Holmes, B. Commeau, A. Arrasmith, L. Cincio, P. J. Coles, and A. Sornborger, Long-time simulations with high fidelity on quantum hardware (2021), arXiv:2102.04313 [quant-ph].

[18] Y.-X. Yao, N. Gomes, F. Zhang, T. Iadecola, C.-Z. Wang, K.-M. Ho, and P. P. Orth, Adaptive variational quantum dynamics simulations, arXiv preprint arXiv:2011.00622 (2020).

[19] H. Lamm, S. Lawrence, and Y. Yamauchi (NuQS), General Methods for Digital Quantum Simulation of Gauge Theories, Phys. Rev. **D100**, 034518 (2019), arXiv:1903.08807 [hep-lat].

[20] M. S. Alam, S. Hadfield, H. Lamm, and A. C. Y. Li (SQMS), Primitive quantum gates for dihedral gauge theories, Phys. Rev. D **105**, 114501 (2022), arXiv:2108.13305 [quant-ph].

[21] M. Carena, H. Lamm, Y.-Y. Li, and W. Liu, Improved Hamiltonians for Quantum Simulations (2022), arXiv:2203.02823 [hep-lat].

[22] E. Zohar, J. I. Cirac, and B. Reznik, Simulating Compact Quantum Electrodynamics with ultracold atoms: Probing confinement and nonperturbative effects, Phys. Rev. Lett. **109**, 125302 (2012), arXiv:1204.6574 [quant-ph].

[23] E. Zohar, J. I. Cirac, and B. Reznik, Cold-Atom Quantum Simulator for SU(2) Yang-Mills Lattice Gauge Theory, Phys. Rev. Lett. **110**, 125304 (2013), arXiv:1211.2241 [quant-ph].

[24] E. Zohar, J. I. Cirac, and B. Reznik, Quantum simulations of gauge theories with ultracold atoms: local gauge invariance from angular momentum conservation, Phys. Rev. **A88**, 023617 (2013), arXiv:1303.5040 [quant-ph].

[25] E. Zohar and M. Burrello, Formulation of lattice gauge theories for quantum simulations, Phys. Rev. **D91**, 054506 (2015), arXiv:1409.3085 [quant-ph].

[26] E. Zohar, J. I. Cirac, and B. Reznik, Quantum Simulations of Lattice Gauge Theories using Ultracold Atoms in Optical Lattices, Rept. Prog. Phys. **79**, 014401 (2016), arXiv:1503.02312 [quant-ph].

[27] E. Zohar, A. Farace, B. Reznik, and J. I. Cirac, Digital lattice gauge theories, Phys. Rev. **A95**, 023604 (2017), arXiv:1607.08121 [quant-ph].

[28] N. Klco, J. R. Stryker, and M. J. Savage, SU(2) non-Abelian gauge field theory in one dimension on digital quantum computers, Phys. Rev. D **101**, 074512 (2020), arXiv:1908.06935 [quant-ph].

[29] A. Ciavarella, N. Klco, and M. J. Savage, A Trailhead for Quantum Simulation of SU(3) Yang-Mills Lattice Gauge Theory in the Local Multiplet Basis (2021), arXiv:2101.10227 [quant-ph].

[30] J. Liu and Y. Xin, Quantum simulation of quantum field

theories as quantum chemistry (2020), arXiv:2004.13234 [hep-th].

[31] D. C. Hackett, K. Howe, C. Hughes, W. Jay, E. T. Neil, and J. N. Simone, Digitizing Gauge Fields: Lattice Monte Carlo Results for Future Quantum Computers, Phys. Rev. A **99**, 062341 (2019), arXiv:1811.03629 [quant-ph].

[32] A. Alexandru, P. F. Bedaque, S. Harmalkar, H. Lamm, S. Lawrence, and N. C. Warrington (NuQS), Gluon field digitization for quantum computers, Phys.Rev.D **100**, 114501 (2019), arXiv:1906.11213 [hep-lat].

[33] A. Yamamoto, Real-time simulation of (2+1)-dimensional lattice gauge theory on qubits, PTEP **2021**, 013B06 (2021), arXiv:2008.11395 [hep-lat].

[34] J. F. Haase, L. Dellantonio, A. Celi, D. Paulson, A. Kan, K. Jansen, and C. A. Muschik, A resource efficient approach for quantum and classical simulations of gauge theories in particle physics, Quantum **5**, 393 (2021), arXiv:2006.14160 [quant-ph].

[35] T. Armon, S. Ashkenazi, G. García-Moreno, A. González-Tudela, and E. Zohar, Photon-mediated Stroboscopic Quantum Simulation of a $\mathbb{Z}_2$ Lattice Gauge Theory (2021), arXiv:2107.13024 [quant-ph].

[36] A. Bazavov, S. Catterall, R. G. Jha, and J. Unmuth-Yockey, Tensor renormalization group study of the non-abelian higgs model in two dimensions, Phys. Rev. D **99**, 114507 (2019).

[37] A. Bazavov, Y. Meurice, S.-W. Tsai, J. Unmuth-Yockey, and J. Zhang, Gauge-invariant implementation of the Abelian Higgs model on optical lattices, Phys. Rev. **D92**, 076003 (2015), arXiv:1503.08354 [hep-lat].

[38] J. Zhang, J. Unmuth-Yockey, J. Zeiher, A. Bazavov, S. W. Tsai, and Y. Meurice, Quantum simulation of the universal features of the Polyakov loop, Phys. Rev. Lett. **121**, 223201 (2018), arXiv:1803.11166 [hep-lat].

[39] J. Unmuth-Yockey, J. Zhang, A. Bazavov, Y. Meurice, and S.-W. Tsai, Universal features of the Abelian Polyakov loop in 1+1 dimensions, Phys. Rev. **D98**, 094511 (2018), arXiv:1807.09186 [hep-lat].

[40] J. F. Unmuth-Yockey, Gauge-invariant rotor Hamiltonian from dual variables of 3D $U(1)$ gauge theory, Phys. Rev. D **99**, 074502 (2019), arXiv:1811.05884 [hep-lat].

[41] M. Kreshchuk, W. M. Kirby, G. Goldstein, H. Beauchemin, and P. J. Love, Quantum Simulation of Quantum Field Theory in the Light-Front Formulation (2020), arXiv:2002.04016 [quant-ph].

[42] M. Kreshchuk, S. Jia, W. M. Kirby, G. Goldstein, J. P. Vary, and P. J. Love, Simulating Hadronic Physics on NISQ devices using Basis Light-Front Quantization (2020), arXiv:2011.13443 [quant-ph].

[43] I. Raychowdhury and J. R. Stryker, Solving Gauss's Law on Digital Quantum Computers with Loop-String-Hadron Digitization (2018), arXiv:1812.07554 [hep-lat].

[44] I. Raychowdhury and J. R. Stryker, Loop, String, and Hadron Dynamics in SU(2) Hamiltonian Lattice Gauge Theories, Phys. Rev. D **101**, 114502 (2020), arXiv:1912.06133 [hep-lat].

[45] Z. Davoudi, I. Raychowdhury, and A. Shaw, Search for Efficient Formulations for Hamiltonian Simulation of non-Abelian Lattice Gauge Theories (2020), arXiv:2009.11802 [hep-lat].

[46] U.-J. Wiese, Towards Quantum Simulating QCD, *Proceedings, 24th International Conference on Ultra-Relativistic Nucleus-Nucleus Collisions (Quark Matter 2014): Darmstadt, Germany, May 19-24, 2014*, Nucl. Phys. **A931**, 246 (2014), arXiv:1409.7414 [hep-th].

[47] D. Luo, J. Shen, M. Highman, B. K. Clark, B. DeMarco, A. X. El-Khadra, and B. Gadway, A Framework for Simulating Gauge Theories with Dipolar Spin Systems (2019), arXiv:1912.11488 [quant-ph].

[48] R. C. Brower, D. Berenstein, and H. Kawai, Lattice Gauge Theory for a Quantum Computer, PoS **LATTICE2019**, 112 (2019), arXiv:2002.10028 [hep-lat].

[49] S. V. Mathis, G. Mazzola, and I. Tavernelli, Toward scalable simulations of Lattice Gauge Theories on quantum computers, Phys. Rev. D **102**, 094501 (2020), arXiv:2005.10271 [quant-ph].

[50] H. Singh, Qubit $O(N)$ nonlinear sigma models (2019), arXiv:1911.12353 [hep-lat].

[51] H. Singh and S. Chandrasekharan, Qubit regularization of the $O(3)$ sigma model, Phys. Rev. D **100**, 054505 (2019), arXiv:1905.13204 [hep-lat].

[52] A. J. Buser, T. Bhattacharya, L. Cincio, and R. Gupta, Quantum simulation of the qubit-regularized O(3)-sigma model (2020), arXiv:2006.15746 [quant-ph].

[53] T. Bhattacharya, A. J. Buser, S. Chandrasekharan, R. Gupta, and H. Singh, Qubit regularization of asymptotic freedom (2020), arXiv:2012.02153 [hep-lat].

[54] J. a. Barata, N. Mueller, A. Tarasov, and R. Venugopalan, Single-particle digitization strategy for quantum computation of a ϕ^4 scalar field theory (2020), arXiv:2012.00020 [hep-th].

[55] M. Kreshchuk, S. Jia, W. M. Kirby, G. Goldstein, J. P. Vary, and P. J. Love, Light-Front Field Theory on Current Quantum Computers (2020), arXiv:2009.07885 [quant-ph].

[56] Y. Ji, H. Lamm, and S. Zhu (NuQS), Gluon Field Digitization via Group Space Decimation for Quantum Computers, Phys. Rev. D **102**, 114513 (2020), arXiv:2005.14221 [hep-lat].

[57] C. W. Bauer and D. M. Grabowska, Efficient Representation for Simulating U(1) Gauge Theories on Digital Quantum Computers at All Values of the Coupling (2021), arXiv:2111.08015 [hep-ph].

[58] E. Gustafson, Prospects for Simulating a Qudit Based Model of (1+1)d Scalar QED, Phys. Rev. D **103**, 114505 (2021), arXiv:2104.10136 [quant-ph].

[59] T. Hartung, T. Jakobs, K. Jansen, J. Ostmeyer, and C. Urbach, Digitising SU(2) gauge fields and the freezing transition, Eur. Phys. J. C **82**, 237 (2022), arXiv:2201.09625 [hep-lat].

[60] D. M. Grabowska, C. Kane, B. Nachman, and C. W. Bauer, Overcoming exponential scaling with system size in Trotter-Suzuki implementations of constrained Hamiltonians: 2+1 U(1) lattice gauge theories (2022), arXiv:2208.03333 [quant-ph].

[61] E. M. Murairi, M. J. Cervia, H. Kumar, P. F. Bedaque, and A. Alexandru, How many quantum gates do gauge theories require? (2022), arXiv:2208.11789 [hep-lat].

[62] P. Hasenfratz and F. Niedermayer, Asymptotic freedom with discrete spin variables?, *Proceedings, 2001 Europhysics Conference on High Energy Physics (EPS-HEP 2001): Budapest, Hungary, July 12-18, 2001*, PoS **HEP2001**, 229 (2001), arXiv:hep-lat/0112003 [hep-lat].

[63] S. Caracciolo, A. Montanari, and A. Pelissetto, Asymptotically free models and discrete nonAbelian groups, Phys. Lett. **B513**, 223 (2001), arXiv:hep-lat/0103017 [hep-lat].

[64] P. Hasenfratz and F. Niedermayer, Asymptotically free theories based on discrete subgroups, *Lattice field theory. Proceedings, 18th International Symposium, Lattice 2000, Bangalore, India, August 17-22, 2000*, Nucl. Phys. Proc. Suppl. **94**, 575 (2001), arXiv:hep-lat/0011056 [hep-lat].

[65] A. Patrascioiu and E. Seiler, Continuum limit of two-dimensional spin models with continuous symmetry and conformal quantum field theory, Phys. Rev. E **57**, 111 (1998).

[66] R. Krcmar, A. Gendiar, and T. Nishino, Phase diagram of a truncated tetrahedral model, Phys. Rev. E **94**, 022134 (2016).

[67] S. Caracciolo, A. Montanari, and A. Pelissetto, Asymptotically free models and discrete non-abelian groups, Physics Letters B **513**, 223 (2001).

[68] J. Zhou, H. Singh, T. Bhattacharya, S. Chandrasekharan, and R. Gupta, Spacetime symmetric qubit regularization of the asymptotically free two-dimensional O(4) model, Phys. Rev. D **105**, 054510 (2022), arXiv:2111.13780 [hep-lat].

[69] S. Caspar and H. Singh, From asymptotic freedom to θ vacua: Qubit embeddings of the O(3) nonlinear σ model (2022), arXiv:2203.15766 [hep-lat].

[70] E. Zohar, Quantum Simulation of Lattice Gauge Theories in more than One Space Dimension – Requirements, Challenges, Methods (2021), arXiv:2106.04609 [quant-ph].

[71] M. Carena, H. Lamm, Y.-Y. Li, and W. Liu, Lattice Renormalization of Quantum Simulations (2021), arXiv:2107.01166 [hep-lat].

[72] D. González-Cuadra, T. V. Zache, J. Carrasco, B. Kraus, and P. Zoller, Hardware efficient quantum simulation of non-abelian gauge theories with qudits on Rydberg platforms (2022), arXiv:2203.15541 [quant-ph].

[73] M. Creutz, L. Jacobs, and C. Rebbi, Monte Carlo Study of Abelian Lattice Gauge Theories, Phys. Rev. **D20**, 1915 (1979).

[74] M. Creutz and M. Okawa, Generalized Actions in $Z(p)$ Lattice Gauge Theory, Nucl. Phys. **B220**, 149 (1983).

[75] G. Bhanot and C. Rebbi, Monte Carlo Simulations of Lattice Models With Finite Subgroups of SU(3) as Gauge Groups, Phys. Rev. **D24**, 3319 (1981).

[76] D. Petcher and D. H. Weingarten, Monte Carlo Calculations and a Model of the Phase Structure for Gauge Theories on Discrete Subgroups of SU(2), Phys. Rev. **D22**, 2465 (1980).

[77] G. Bhanot, SU(3) Lattice Gauge Theory in Four-dimensions With a Modified Wilson Action, Phys. Lett. **108B**, 337 (1982).

[78] Y. Ji, H. Lamm, and S. Zhu, Gluon Digitization via Character Expansion for Quantum Computers (2022), arXiv:2203.02330 [hep-lat].

[79] A. Alexandru, P. F. Bedaque, R. Brett, and H. Lamm, The spectrum of qubitized QCD: glueballs in a $S(1080)$ gauge theory (2021), arXiv:2112.08482 [hep-lat].

[80] M. Carena, E. J. Gustafson, H. Lamm, Y.-Y. Li, and W. Liu, Gauge Theory Couplings on Anisotropic Lattices (2022), arXiv:2208.10417 [hep-lat].

[81] D. H. Weingarten and D. N. Petcher, Monte Carlo Integration for Lattice Gauge Theories with Fermions, Phys. Lett. **99B**, 333 (1981).

[82] D. Weingarten, Monte Carlo Evaluation of Hadron Masses in Lattice Gauge Theories with Fermions, Phys. Lett. **109B**, 57 (1982), [,631(1981)].

[83] J. B. Kogut, 1/n Expansions and the Phase Diagram of Discrete Lattice Gauge Theories With Matter Fields, Phys. Rev. D **21**, 2316 (1980).

[84] J. Romers, *Discrete gauge theories in two spatial dimensions*, Ph.D. thesis, Master's thesis, Universiteit van Amsterdam (2007).

[85] E. H. Fradkin and S. H. Shenker, Phase Diagrams of Lattice Gauge Theories with Higgs Fields, Phys. Rev. D **19**, 3682 (1979).

[86] D. Harlow and H. Ooguri, Symmetries in quantum field theory and quantum gravity (2018), arXiv:1810.05338 [hep-th].

[87] D. Horn, M. Weinstein, and S. Yankielowicz, Hamiltonian Approach to Z(N) Lattice Gauge Theories, Phys. Rev. D **19**, 3715 (1979).

[88] M. Fromm, O. Philipsen, and C. Winterowd, Dihedral Lattice Gauge Theories on a Quantum Annealer (2022), arXiv:2206.14679 [hep-lat].

[89] M. S. Alam *et al.*, Quantum computing hardware for HEP algorithms and sensing, in *2022 Snowmass Summer Study* (2022) arXiv:2204.08605 [quant-ph].

[90] T. Fösel, S. Krastanov, F. Marquardt, and L. Jiang, Efficient cavity control with snap gates (2020).

[91] R. W. Heeres, B. Vlastakis, E. Holland, S. Krastanov, V. V. Albert, L. Frunzio, L. Jiang, and R. J. Schoelkopf, Cavity state manipulation using photon-number selective phase gates, Physical Review Letters **115**, 10.1103/physrevlett.115.137002 (2015).

[92] S. Krastanov, V. V. Albert, C. Shen, C.-L. Zou, R. W. Heeres, B. Vlastakis, R. J. Schoelkopf, and L. Jiang, Universal control of an oscillator with dispersive coupling to a qubit, Physical Review A **92**, 10.1103/physreva.92.040303 (2015).

[93] S. Chakram, K. He, A. V. Dixit, A. E. Oriani, R. K. Naik, N. Leung, H. Kwon, W.-L. Ma, L. Jiang, and D. I. Schuster, Multimode photon blockade, Nature Physics , 1 (2022).

[94] K. Hou, C. J. Zhu, Y. P. Yang, and G. S. Agarwal, Interfering pathways for photon blockade in cavity QED with one and two qubits, Phys. Rev. A **100**, 063817 (2019), arXiv:1907.05997 [quant-ph].

[95] S. Chakram, A. E. Oriani, R. K. Naik, A. V. Dixit, K. He, A. Agrawal, H. Kwon, and D. I. Schuster, Seamless high-q microwave cavities for multimode circuit quantum electrodynamics, Phys. Rev. Lett. **127**, 107701 (2021).

[96] J. P. Palao and R. Kosloff, Quantum computing by an optimal control algorithm for unitary transformations, Phys. Rev. Lett. **89**, 188301 (2002).

[97] N. A. Petersson and F. Garcia, Optimal control of closed quantum systems via b-splines with carrier waves (2021).

[98] A. B. Özgüler and D. Venturelli, Numerical Gate Synthesis for Quantum Heuristics on Bosonic Quantum Processors (2022), arXiv:2201.07787 [quant-ph].

[99] A. Barış Özgüler and J. A. Job, Dynamics of qudit gates and effects of spectator modes on optimal control pulses (2022), arXiv:2207.14006 [quant-ph].

[100] M. A. Nielsen and I. L. Chuang, *Quantum Computation and Quantum Information: 10th Anniversary Edition* (Cambridge University Press, 2010).

[101] P. Hoyer, Efficient quantum transforms, arXiv preprint quant-ph/9702028 (1997).

[102] R. Beals, Quantum computation of Fourier transforms over symmetric groups, in *Proceedings of the twenty-ninth annual ACM symposium on Theory of computing*

(Citeseer, 1997) pp. 48–53.

[103] M. Püschel, M. Rötteler, and T. Beth, Fast quantum Fourier transforms for a class of non-abelian groups, in *International Symposium on Applied Algebra, Algebraic Algorithms, and Error-Correcting Codes* (Springer, 1999) pp. 148–159.

[104] C. Moore, D. Rockmore, and A. Russell, Generic quantum Fourier transforms, ACM Transactions on Algorithms (TALG) **2**, 707 (2006).

[105] A. M. Childs and W. Van Dam, Quantum algorithms for algebraic problems, Reviews of Modern Physics **82**, 1 (2010).

[106] F. Shah Khan and M. Perkowski, Synthesis of multi-qudit Hybrid and d-valued Quantum Logic Circuits by Decomposition, arXiv e-prints , quant-ph/0511019 (2005), arXiv:quant-ph/0511019 [quant-ph].

[107] I. L. Chuang and M. A. Nielsen, Prescription for experimental determination of the dynamics of a quantum black box, J. Mod. Opt. **44**, 2455 (1997), arXiv:quant-ph/9610001.

[108] A. Erhard, J. J. Wallman, L. Postler, M. Meth, R. Stricker, E. A. Martinez, P. Schindler, T. Monz, J. Emerson, and R. Blatt, Characterizing large-scale quantum computers via cycle benchmarking, Nature Communications **10**, 10.1038/s41467-019-13068-7 (2019).

[109] Y. Li and S. C. Benjamin, Efficient variational quantum simulator incorporating active error minimization, Physical Review X **7**, 021050 (2017).

[110] S. Endo, S. C. Benjamin, and Y. Li, Practical quantum error mitigation for near-future applications, Physical Review X **8**, 10.1103/physrevx.8.031027 (2018).

[111] M. R. Geller and Z. Zhou, Efficient error models for fault-tolerant architectures and the pauli twirling approximation, Physical Review A **88**, 10.1103/physreva.88.012314 (2013).

[112] J. J. Wallman and J. Emerson, Noise tailoring for scalable quantum computation via randomized compiling, Physical Review A **94**, 10.1103/physreva.94.052325 (2016).

[113] K. Yeter-Aydeniz, Z. Parks, A. Nair, E. Gustafson, A. F. Kemper, R. C. Pooser, Y. Meurice, and P. Dreher, Measuring NISQ Gate-Based Qubit Stability Using a 1+1 Field Theory and Cycle Benchmarking (2022), arXiv:2201.02899 [quant-ph].

[114] B. Eastin and E. Knill, Restrictions on transversal encoded quantum gate sets, Physical Review Letters **102**, 10.1103/physrevlett.102.110502 (2009).

[115] A. R. Calderbank and P. W. Shor, Good quantum error-correcting codes exist, Phys. Rev. A **54**, 1098 (1996), arXiv:quant-ph/9512032 [quant-ph].

[116] A. M. Steane, Error correcting codes in quantum theory, Phys. Rev. Lett. **77**, 793 (1996).

[117] A. Steane, Multiple-Particle Interference and Quantum Error Correction, Proceedings of the Royal Society of London Series A **452**, 2551 (1996), arXiv:quant-ph/9601029 [quant-ph].

[118] A. M. Steane, Simple quantum error-correcting codes, Phys. Rev. A **54**, 4741 (1996).

[119] A. Y. Kitaev, Quantum computations: algorithms and error correction, Russian Mathematical Surveys **52**, 1191 (1997).

[120] A. Barenco, C. H. Bennett, R. Cleve, D. P. DiVincenzo, N. Margolus, P. Shor, T. Sleator, J. A. Smolin, and

H. Weinfurter, Elementary gates for quantum computation, Phys. Rev. A **52**, 3457 (1995).

[121] J. M. Baker, C. Duckering, A. Hoover, and F. T. Chong, Decomposing Quantum Generalized Toffoli with an Arbitrary Number of Ancilla, arXiv e-prints , arXiv:1904.01671 (2019), arXiv:1904.01671 [quant-ph].

[122] A. Bocharov, M. Roetteler, and K. M. Svore, Efficient synthesis of universal repeat-until-success quantum circuits, Phys. Rev. Lett. **114**, 080502 (2015).

[123] T. D. Cohen, H. Lamm, S. Lawrence, and Y. Yamauchi (NuQS), Quantum algorithms for transport coefficients in gauge theories, Phys. Rev. D **104**, 094514 (2021), arXiv:2104.02024 [hep-lat].

[124] A. Kan and Y. Nam, Lattice Quantum Chromodynamics and Electrodynamics on a Universal Quantum Computer (2021), arXiv:2107.12769 [quant-ph].

[125] A. Ashikhmin and E. Knill, Nonbinary quantum stabilizer codes, IEEE Transactions on Information Theory **47**, 3065 (2001).

[126] A. Ketkar, A. Klappenecker, S. Kumar, and P. Sarvepalli, Nonbinary stabilizer codes over finite fields, IEEE Transactions on Information Theory **52**, 4892 (2006).

[127] L. Luo, Z. Ma, Z. Wei, and R. Leng, Non-binary entanglement-assisted quantum stabilizer codes, Science China Information Sciences **60**, 1 (2017).

[128] C. Galindo, F. Hernando, R. Matsumoto, and D. Ruano, Entanglement-assisted quantum error-correcting codes over arbitrary finite fields, Quantum Information Processing **18**, 1 (2019).

[129] P. J. Nadkarni and S. S. Garani, Coding analog of superadditivity using entanglement-assisted quantum tensor product codes over $\mathbb{F}_{p^k}$, IEEE Transactions on Quantum Engineering **1**, 1 (2020).

[130] G. M. Nikolopoulos, K. S. Ranade, and G. Alber, Error tolerance of two-basis quantum-key-distribution protocols using qudits and two-way classical communication, Phys. Rev. A **73**, 032325 (2006).

[131] P. Imany, J. A. Jaramillo-Villegas, M. S. Alshaykh, J. M. Lukens, O. D. Odele, A. J. Moore, D. E. Leaird, M. Qi, and A. M. Weiner, High-dimensional optical quantum logic in large operational spaces, npj Quantum Information **5**, 1 (2019).

[132] R. Majumdar and S. Sur-Kolay, Optimal error correcting code for ternary quantum systems (2019).

[133] C. Galindo, F. Hernando, R. Matsumoto, and D. Ruano, Asymmetric entanglement-assisted quantum error-correcting codes and BCH codes, IEEE Access **8**, 18571 (2020).

[134] P. J. Nadkarni and S. S. Garani, Quantum error correction architecture for qudit stabilizer codes, Phys. Rev. A **103**, 042420 (2021).

[135] R. Majumdar and S. Sur-Kolay, Exploiting degeneracy to construct good ternary quantum error correcting code (2020).

[136] M. Chizzini, L. Crippa, L. Zaccardi, E. Macaluso, S. Carretta, A. Chiesa, and P. Santini, Quantum error correction with molecular spin qudits, Physical Chemistry Chemical Physics (2022).

[137] R. Majumdar, S. Basu, S. Ghosh, and S. Sur-Kolay, Quantum error-correcting code for ternary logic, Phys. Rev. A **97**, 052302 (2018).

[138] A. Glaudell, N. J. Ross, J. van de Wetering, and L. Yeh, Qutrit metaplectic gates are a subset of clifford+t (2022).

[139] R. R. Vandermolen and D. Wright, Graph-theoretic ap-

proach to quantum error correction, Phys. Rev. A **105**, 032450 (2022), arXiv:2110.08414 [quant-ph].

[140] T. Tilma and E. C. G. Sudarshan, Generalized Euler angle parametrization for SU(N), Journal of Physics A Mathematical General **35**, 10467 (2002), arXiv:math-ph/0205016 [math-ph].

[141] S. Bertini, S. L. Cacciatori, and B. L. Cerchiai, On the Euler angles for SU(N), Journal of Mathematical Physics **47**, 043510 (2006), arXiv:math-ph/0510075 [math-ph].

[142] T. Tilma and E. C. G. Sudarshan, Generalized Euler angle parameterization for U(N) with applications to SU(N) coset volume measures, Journal of Geometry and Physics **52**, 263 (2004), arXiv:math-ph/0210057 [math-ph].

Appendix A: SU(N) Euler angle decompositions

The following operators $\mathcal{U}_2^{(a,b)}$, $\mathcal{U}_3^{(a,b,c)}$, $\mathcal{U}_4^{(a,b,c,d)}$, and $\mathcal{U}_6^{(a,b,c,d,e,f)}$ correspond to specific $SU(N)$ rotations that implement the $QFT_{\mathbb{Z}_m}$ of Tab. II. We use the following Euler angle decompositions where the superscripts indicate levels that are swapped between. The $SU(2)$ Euler angle decomposition we require is built from the well-known ZXZ rotation

$$\mathcal{U}_2^{(a,b)}(\vec{\theta}_{II}) = R_Z^{(a,b)}(\theta_0)R_X^{(a,b)}(\theta_1)R_Z^{(a,b)}(\theta_2). \quad (A1)$$

For the two-state rotation we need, $\vec{\theta}_{II} = [\pi/2, \pi/2, \pi/2]$. An example of the operator V_g with cycle $m = 2$ would be for $g = -\mathbb{1}$, which corresponds to $|1\rangle$, and is given by:

$$V_1 = \prod_{a=0}^{11} \mathcal{U}_2^{(2a,2a+1)}(\vec{\theta}_{II}). \quad (A2)$$

The $SU(3)$ Euler angle decomposition requires two $\mathcal{U}_2^{(a,b)}(\vec{\theta})$ and two Givens rotations [106, 140–142],

$$\mathcal{U}_3^{(a,b,c)}(\vec{\theta}_{III}) = \mathcal{U}_2^{(a,b)}(\vec{\theta}_0)R_X^{(b,c)}(\theta_1)\mathcal{U}_2^{(a,b)}(\vec{\theta}_2)R_Z^{(b,c)}(\theta_3), \quad (A3)$$

where the angles are fixed to: $\vec{\theta}_0 = [7\pi/6, 3\pi/2, \pi/2]$, $\theta_1 = 0.608175\pi$, $\vec{\theta}_4 = [0, -\pi/2, \pi/3]$, $\theta_3 = 7\pi/3$. One element with $m = 3$ is $g = \mathbf{l}$, corresponding to $|8\rangle$:

$$V_8 = \prod_{a=0}^{7} \mathcal{U}_3^{(a,a+8,a+16)}(\vec{\theta}_{III}). \quad (A4)$$

The Euler angle decomposition of an arbitrary $SU(4)$ is given in terms of three $\mathcal{U}_2^{(a,b)}(\vec{\theta})$ and six Givens rotations

$$\begin{aligned}\mathcal{U}_4^{(a,b,c,d)}(\vec{\theta}_{IV}) =& \mathcal{U}_2^{(a,b)}(\vec{\theta}_0)R_X^{(b,c)}(\theta_1)R_Z^{(a,b)}(\theta_2) \\ & R_Z^{(c,d)}(\theta_3)\mathcal{U}_2^{(a,b)}(\vec{\theta}_4)R_X^{(b,c)}(\theta_5) \\ & \mathcal{U}_2^{(a,b)}(\vec{\theta}_6)R_Z^{(b,c)}(\theta_7)R_Z^{(c,d)}(\theta_8),\end{aligned} \quad (A5)$$

where the angles required for $QFT_{\mathbb{Z}_4}$ are fixed to be: $\vec{\theta}_0 = [2\pi, \pi/2, 0]$, $\theta_1 = 1.392\pi$, $\theta_2 = 0.4511\pi$, $\theta_3 = 4\pi/3$, $\vec{\theta}_4 = [0.90126\pi, 0.41956\pi, 1.852\pi]$, $\theta_5 = 0.60817\pi$, $\vec{\theta}_6 = [\pi/2, \pi/4, -\pi/4]$, $\theta_7 = -\pi/2$, $\theta_8 = -3\pi/4$. If we consider the example $g = \mathbf{i}$, $(|2\rangle)$ then V_2 would be:

$$V_2 = \prod_{a=0}^{5} \mathcal{U}_4^{(4a,4a+2,4a+1,4a+3)}(\vec{\theta}_{IV}). \quad (A6)$$

The final decomposition required for $\mathbb{BT}$ is $SU(6)$, which is given by two $\mathcal{U}_3^{(a,b,c)}(\vec{\theta})$ and three $\mathcal{U}_2^{(a,b)}(\vec{\theta}_0)$:

$$\begin{aligned}\mathcal{U}_6^{(a,b,c,d,e,f)} =& \mathcal{U}_3^{(a,b,c)}(\vec{\theta}_{III})\mathcal{U}_3^{(d,e,f)}(\vec{\theta}_{III}) \\ & \times \mathcal{U}_2^{(a,d)}(\vec{\theta}_{II})\mathcal{U}_2^{(b,e)}(\vec{\theta}_{II})\mathcal{U}_2^{(c,f)}(\vec{\theta}_{II}).\end{aligned} \quad (A7)$$

The group element $-\mathbf{l}$ corresponding to $|9\rangle$ has order $m = 6$. The corresponding V_9 is made with four products of $\mathcal{U}_6^{(a,b,c,d,e,f)}$, although it lacks the obvious structure of the other examples shown thus far:

$$\begin{aligned}V_9 =& \mathcal{U}_6^{(0,9,16,1,8,17)}\mathcal{U}_6^{(2,14,20,3,15,21)} \\ & \mathcal{U}_6^{(4,11,23,5,10,22)}\mathcal{U}_6^{(6,12,19,7,13,18)}.\end{aligned} \quad (A8)$$